Progress in Additive Manufacturing
https://doi.org/10.1007/s40964-024-00696-9

FULL RESEARCH ARTICLE

Screw extrusion additive manufacturing of thermoplastic polyolefin elastomer

Albert Curmi[1] · **Arif Rochman**[1] · **Alfred Gatt**[2]

Received: 2 April 2024 / Accepted: 4 June 2024

Abstract

This study determined the requisite process parameters for good-quality screw extrusion additive manufacturing (AM) of thermoplastic polyolefin (TPO) using fused granulate fabrication (FGF). TPO is a non-hygroscopic, cheaper, and less dense alternative to the well-established thermoplastic polyurethane (TPU). TPO was found to extrude correctly at 170 °C, on a glass build plate at 80 °C with Magigoo PP adhesive. A water uptake test on TPO reported a mass gain plateau of 0.25%, which is significantly lower than that of TPU, which suggests that TPO may not require drying before 3D printing. Tensile testing on FGF TPO specimens achieved similar stress at yield as well as stress and strain at break as indicated by the data sheet for the XY and YZ orientations. The Z direction is significantly weaker than the X and Y orientations, reaching only 30% of the stress at break. TPO achieved the best average stress at yield of 6.36 MPa using the 0.4 mm nozzle with XY printing orientation and stress and strain at break of 13.8 MPa and 1300% at YZ orientation and 1 mm nozzle. The setup achieved relatively high-quality prints of complex geometries, including the popular torture-test Benchy and a child-sized orthotic insole.

Keywords Material extrusion · Screw extrusion · Fused granular fabrication (FGF) · Thermoplastic elastomer (TPE) · Thermoplastic polyolefin elastomer (TPO)

1 Introduction

Thermoplastic polyolefin (TPO) is the second most used thermoplastic elastomer (TPE), just after styrenic TPE, taking up 26% of the share. It is used in automotive, consumer goods, asphalt, roofing, adhesives, sealants, and coatings [1]. TPO is also inexpensive; in fact, its largest market is the automotive sector. It is often selected for its low cost, low-temperature toughness, weatherability, and low specific gravity [2]. Despite its wide application, TPO has not been widely studied for material extrusion (MEX) additive manufacturing (AM), especially with screw extrusion, fused granulate fabrication (FGF).

The first study that employed TPO for MEX AM was published by Laoutid et al. which managed to 3D print TPO-rubber blends using fused filament fabrication (FFF). The group achieved good-quality 3D prints; however, the 3D-printed geometries were not complex [3]. Another study using FFF was carried out by Lv et al. which 3D printed TPO with graphene nanoplatelets. This nanocomposite was used to 3D print products with improved electromagnetic shielding performance [4]. The first study involving FFF 3D printing of unfilled TPO grades was conducted by Adrover-Monserrat et al. which evaluated the mechanical properties achievable using this material. The study reported a yield strength of 3.4 MPa and a maximum stress of 4.5 MPa at a strain at failure of 350%, when tensile testing along the extrudate direction [5].

The principal advantage of TPO over the current dominant MEX elastomer, i.e., thermoplastic polyurethane (TPU), is TPO's non-hygroscopic nature. No pre-drying should be necessary prior to 3D printing when using TPO pellets or even filament [6]. Humidity absorption in

✉ Arif Rochman
arif.rochman@um.edu.mt

Albert Curmi
albert.curmi.98@gmail.com

Alfred Gatt
alfred.gatt@um.edu.mt

[1] Department of Industrial and Manufacturing Engineering, University of Malta, Msida 2080, Malta

[2] Department of Podiatry, University of Malta, Msida 2080, Malta

Published online: 15 June 2024

TPU causes bubbles in the 3D-printed parts which in turn decreases the aesthetic value and mechanical performance of the product [7]. This advantage alone provides ample reason to study the application of TPO to material extrusion AM as it could significantly decrease the running costs and waste of elastomer MEX AM. Decreasing the need for preparation along with the necessary equipment required for pre-drying would make elastomer MEX AM simpler, more reliable, and less time-consuming. This in turn would make it more approachable for a wider user base.

Apart from the principal advantage of being non-hygroscopic, TPO also has a high impact strength and is light weight [8]. The density of TPO is reported to be 0.88 g/cm^3 [9], whereas, generally speaking, the density of TPU varies from 1.18 up to 1.42 g/cm^3 [10]. TPO also has good chemical resistance, similar to that of polypropylene (PP), and is easy to recycle [8]. The properties of TPO can vary as it is a tunable elastomer composed out of two main components: a polyolefin semi-crystalline thermoplastic and an amorphous elastomeric component. Commonly, TPO is a mixture of isostatic PP and ethylene–propylene random copolymer (EPM). Depending on the ratio of these two components, the hardness and stiffness of the TPO can be altered as desired, customarily ranging from 70 shore A to 70 shore D. The mixture may be made by either mechanically blending the two components or else by dynamic vulcanization [6].

TPO may also be produced via a reactor process which produces an alloy rather than a simple blend [11]. An alloy is a blend between two or more immiscible components which have been compatibilized. In this context, compatibilization means to modify the interfacial properties of one or more components of the blend to stabilize the dispersed components [12]. Reactor processes produce a cheaper TPO than mechanical blending processes, making TPO more affordable [13]. Reactor TPOs also have an improved weldability [11], melt flow, a finer dispersion, and an often more homogenous mixture of the components which stabilizes the properties of the material, when compared with TPO produced using the previously mentioned processes [6]. All the aforementioned attributes make reactor TPO the most amenable version for MEX AM.

Despite the wide application of reactor TPO in multiple sectors, there are no studies that 3D printed TPO using screw extrusion FGF. This technique is more adept for printing elastomers compared to FFF as it does not suffer from filament buckling. A properly calibrated FGF system should therefore produce better quality prints. FGF using elastomers was first studied by Kumar et al. which managed to 3D-printed ethylene vinyl acetate (EVA) elastomer. All 3D-printed parts were rather simple, thickened 2D profiles [14–16]. Complex 3D parts were then direct pellet 3D printed by Leng et al. using TPU granules, including a porous cube and an orthotic insole [17]. A different approach was pioneered by Khondoker et al. which used a large, fixed screw extruder, connected by a heated hose to the moving deposition head. The system was capable of working with styrene-ethylene/butylene-styrene (SEBS) with good results, fabricating complex, elastomeric 3D objects [18].

To produce good-quality 3D-printed elastomeric parts, the correct process parameters are necessary especially in the context of screw extrusion FGF of TPO. Missing information includes the optimal build plate setup, extrusion rate calibration, extruder temperature, retraction settings, and material storage characteristics. Likewise, the mechanical strength of 3D-printed TPO is also poorly understood, especially when using FGF with different nozzle sizes.

This study will determine whether TPO is a suitable material for screw extrusion FGF. As a first step, the FGF process parameters have to be obtained and the 3D-printed quality must be optimized. The next step is to determine the mechanical properties achievable using this process, even along the layer bond. To satisfy the former step, the optimal extruder temperature, build plate surface type and temperature and extrusion rate control were all established. Using the optimized process settings, a set of complex geometries will be 3D printed to analyze the quality achievable with TPO FGF. The mechanical properties of these prints were also evaluated with the aim of understanding the elastomeric temperature range of TPO and its strength. Finally, the principal advantage of TPO, i.e., its non-hygroscopic nature, will also be studied to assess its effect on AM. This study provides an overview of the performance of TPO as an FGF material, identifies a set of process parameters that can enable high-quality 3D printing, and explores the achievable product strength.

2 Materials and methods

2.1 Materials and equipments

The TPO used in this study is a reactor TPO produced by Lyondellbasel, Netherlands with tradename Adflex X 100 G which was delivered in granulate form. The granules were fed to an in-house developed pellet extruder, mounted on a Creality (China), CR-10s 3D printer, shown in Fig. 1. The extruder used an 85 mm long, 20 mm diameter, variable depth, and variable helix angle screw. The screw had three distinct zones, as a standard extrusion screw, namely comprising of feeding, compression and metering zoning, the details of which are listed in Table 1. A similar screw geometry and setup was used in a previous study conducted by Curmi et al. when using polyether ether ketone (PEEK) [19].

The extruder has a single heated zone which directly covers the compression zone, as can be seen in the extruder cross-section of Fig. 1b. The feeding end is water cooled,

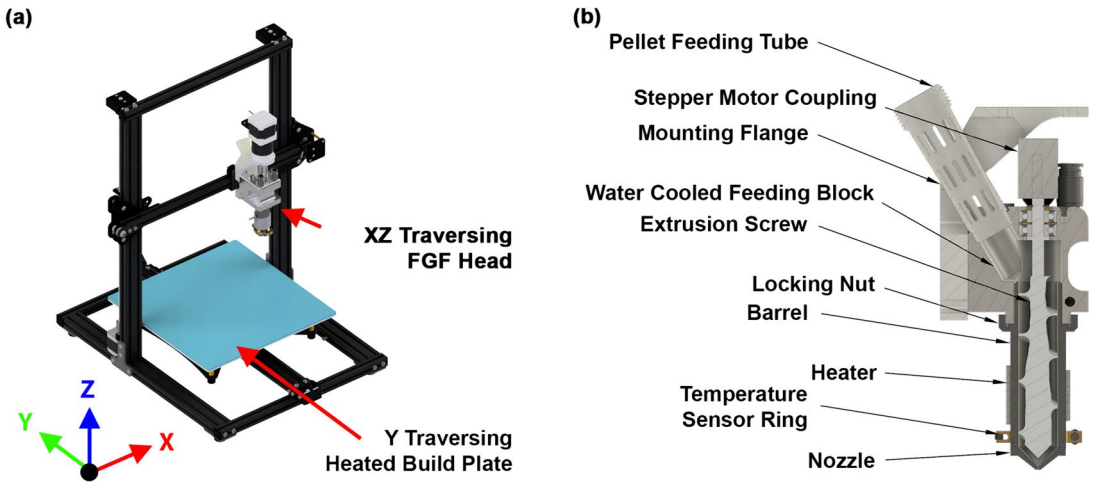

Fig. 1 Renders of (**a**) modified CR-10 s with FGF extruder and (**b**) cross-section and detailed view of FGF extruder

Table 1 Screw geometrical specifications

Screw section	Length [mm]	Turns	Helix angle [°]	Depth [mm]
Feeding	20	1.00	17.67	6.0
Compression	43.75	–	–	–
Metering	21.25	0.82	22.5	3.4

so that a solid feeding zone is created at the start of the extruder. This zone generates most of the pressure developed by the screw [20, 21]. The temperature is measured by a PT100 temperature sensor mounted on the brass ring, as shown in Fig. 1b. A PID temperature control system is used to set the temperature of the barrel to the target temperature. A geared 30:1 NEMA 17 stepper motor 17HS15-1684S-HG30 from Stepper Online (Jiangning Nanjing, China) was used to drive the screw extruder. Two nozzles with diameters of 1 mm and 0.4 mm, respectively, were used throughout this study.

2.2 Differential scanning calorimetry (DSC)

A differential scanning calorimetry (DSC) test was conducted on the TPO granules to determine whether the thermoplastic is amorphous or semi-crystalline, along with the glass transition temperature (T_g), melting temperature (T_m), and the crystallization temperature (T_c). This information is useful both to initially determine an acceptable processing temperature as well as aid in the selection of the temperature for the heated bed [22]. The DSC test was carried out using the raw pellets on a STAR System DSC 3 + by Mettler Toledo (Ohio, USA). The specimen was first heated from room temperature to 200 °C, then cooled to − 100 °C, and heated again to 200 °C, each time at 10 K/min heating and cooling rate, respectively. The test was carried out twice, and in each case, the specimen was kept in a nitrogen atmosphere.

2.3 Determination of FGF process parameters

Unlike filament extruders, screw extruders are not volumetric. Filament extruders assume that the filament being fed has a consistent diameter and therefore can compute the volume being extruder based solely on the length of filament being pushed. Screw extruders on the other hand are not volumetric and therefore the extrusion rate profile of a given extruder must be determined to maintain a consistent output.

To determine the extrusion rate behavior of TPO within this study's setup, an extrusion rate test was conducted. The extruder was gravity-fed TPO pellets and set to extrude. The barrel temperature was first tested at the melting temperature as determined by the DSC test. Subsequently, the temperature was increased in steps of 10 °C until the stepper motor could drive the extruder screw. The extrusion rate was then tested from 160 to 190 °C, in steps of 10 °C. In each case, the extruder speed was varied in between 1 and 9 RPM in steps of 2. The extrusion rate was determined by extruding for 1 min, with 5 repeats, for each testing condition. The extrudates were then weighted on a MYA 11.4Y Plus micro balance, by RADWAG Balances and Scales (Poland).

The calibration of the extruder was carried out by 3D-printing 25 mm-sided cubes using different extrusion multipliers. The extrusion multiplier (EM), also known as flow rate multiplier, was used to account for the non-volumetric nature of screw extrusion 3D printing. The EM was increased or decreased if the cube's dimension were under or over the nominal value. The process was repeated a number of times, until the dimensional accuracy was within 0.1 mm range. The EM was determined for 30 mm/s 3D printing, at the selected 3D-printing temperature, using both 0.4 mm

and 1 mm nozzles. This speed was selected as it assures a good 3D-printing quality, even though the 3D part itself may be too soft to maintain its shape during 3D printing, as the nozzle deposits a subsequent layer.

There is no published method that describes what build plate configuration to use with TPO. Build plate adhesion is a combination of build plate material, coating, and its temperature. To determine a suitable configuration, aluminum sheets, galvanized sheet metal, and glass were tested out using different finishes and temperatures. Both aluminum and galvanized sheet metal were tested out using both a smooth and roughened surface. In the case of glass, this was tested using multiple surface modifications, namely: clean glass; with PEI tape; with PEI tape and PVA glue; with PVA glue; with Magigoo Flex glue and finally with Magigoo PP glue. In each case, the bed was tested once at room temperature and once heated. The heated bed temperature was to be just a bit higher than the T_g of TPO, which was determined by the DSC test. This was done to obtain a good bed adhesion as suggested by Spoerk et al. when studying how to improve PLA and ABS bed adhesion. When the bed temperature is higher than the T_g, the surface tension between the bed and part is reduced and the contact surface area is increased thus improving the bond strength [22].

2.4 3D printing of complex geometries.

The calibrated FGF system was used to 3D print a set of complex geometries. These parts are meant to demonstrate what level of part complexity and quality can be achieved by FGF using TPO. For the purposes of this study, a complex geometry is any model which can be 3D printed without using supports, except for simple, extruded 2D profile. A set of complex models, shown in Fig. 2, were used to both demonstrate the capabilities of the system as well as improve the gcode slicer 3D-printing profile. For this study, the open-source Prusa Slicer (v2.5.0) by Prusa Research was used to generate the gcode to 3D print the models. All models were printed using the 0.4 mm nozzle.

The objectives behind each chosen model are listed summarily in Table 2. The curly vase, shown in Fig. 2 (a), printed in vase mode which disregards the internal volume of the part and prints the outer walls in one continuous spiral. During this process, there are no retractions or otherwise any stops in flow therefore any discontinuities should be easily visible as defects. The iterated curls of the vase are useful to judge if any defects present are caused by the incorrect motion rather than extrusion. A defect which is related to the motion system should be visible as a gradual change across the rotation of the part.

The curly vase served as a steppingstone to then follow up with more complex models, such as the Benchy torture test, shown in Fig. 2c [23]. This model checks for surface, overhangs, and bridging quality as well as dimensional accuracy and propensity for stringing. All of these tests are presented in an aesthetic model, representative of a conventional 3D-printing process. A feature of note are the four corner walls which are supporting the roof. The positioning of these walls causes a stringing and retraction test. Stringing refers to the cobweb of extra, unintended extrudate left on a 3D-printed part. In filament systems, retractions are used to stop the flow of material by pulling the filament and thus depressurizing the hot end. In screw extruders, the same retraction effect can be achieved by simply reversing the extruder screw rotation by some angle. Since Prusa Slicer is meant for filament, the software uses retractions in

Table 2 Models for 3D printing and related objective

Model	Objective
Curly vase	Extrusion rate consistency
Benchy	Retraction testing, lengths: 0 mm; 0.2 mm; 0.5 mm; 1 mm; , which is equivalent to: 0°; 1.2°; 3°; 6°; of screw rotation
Gyroid egg	Retractions' demonstration
Orthotic insole	Application demonstration

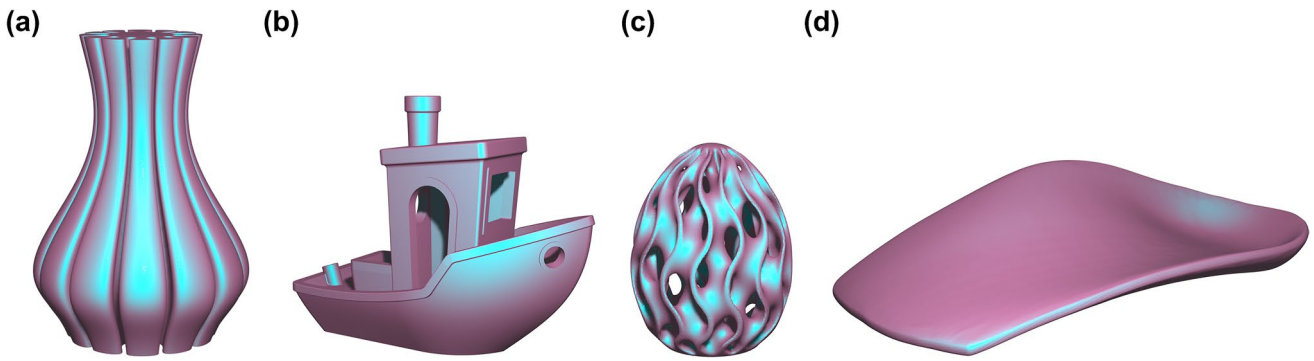

Fig. 2 3D models of: (**a**) curly vase, (**b**) Benchy [23], (**c**) gyroid egg, and (**d**) orthothic insole

millimetres. Therefore, an equivalent value is given for the desired rotation, to achieve the same effect. The Benchy was printed multiple times to calibrate the retraction settings. The retraction angle was tested at 0°, 1.2°, 3°, and 6° of screw rotation.

An even more challenging retraction test then the Benchy, is the gyroid egg [24]. This model is in effect a combination of ordered, twisting columns, which makes for multiple retractions per layer. Therefore, the gyroid egg was printed with optimal settings, using the results of the Benchy torture test to demonstrate the capabilities of the system during an aesthetic 3D print. This model was selected for this study, not just for its value as a retraction test but also as a demonstration of the aesthetic quality achievable by an FGF TPO part.

The optimized pellet 3D-printing system was finally applied to 3D print an orthotic insole. Insoles often need to be customized to a patients' form and therefore can make use of the flexibility provided by 3D printing. The elastomeric nature of TPO makes it a good candidate process for orthotic insole production. Another convenient feature of TPO is its non-hygroscopic nature which may be a useful feature when applied to sweaty environments such as in shoes.

2.5 Characterization of 3D-printed TPO

2.5.1 Water uptake analysis

One of the most notable purported advantages of TPO is its non-hygroscopic nature. A water uptake test was conducted following the *Plastics—Determination of water absorption* DIN EN ISO 62 standard, to determine the water absorption of this grade of TPO. The test was carried out using three 25 mm-long strands of extruded TPO, using the 1 mm nozzle. The strands were produced out of TPO pellets which were dried in a pellet drier for 4 h at 70 °C. The test strands were placed in an airtight container filled with deionized water, and left at a temperature of 23 °C. The test was carried over a period of 16 days, as outlined by the standard. On allocated days, the test strands were collected out of the water, dried using paper towels, and then weighted on a MYA 11.4Y Plus micro balance, by RADWAG Balances and Scales (Poland).

The result of the mass measurements was then fitted using the ideal model of Fick's second law, assuming constant water absorption properties over the diameter of the strands. The model defines the time-dependent water content as shown in Eq. 1, where c_s is the water absorption at saturation (mass %), D is the water diffusion coefficient at the surface normal direction (mm^2/s), d is the strand diameter, t is the duration of immersion time in water (s), and k is index of summation

$$c(t) = c_s\left(1 - \frac{8}{\pi^2}\right)\sum_{k=1}^{20}\frac{1}{(2k-1)^2}e^{\left[-\frac{(2k-1)^2 D\pi^2 t}{d^2}\right]}. \quad (1)$$

The water diffusion coefficient was estimated using Eq. 2, where t_{70} is the time at which the strand reached 70% saturation

$$D = \frac{d^2}{\pi^2 t_{70}}. \quad (2)$$

2.5.2 Tensile testing

Tensile testing was carried out to determine the strain as well as the stress at yield and stress at break of FGF TPO. These properties allow for informed mechanical design of simple loading scenarios of any component to be 3D printed out of TPO. The specimens were designed using the *Standard Test Methods for Vulcanized Rubber and Thermoplastic Elastomers-Tension*, ASTM D412-06A standard, type C shape, and printed 2 mm thick. Since such a standard is not intended for 3D printing, it does not account for any possible anisotropy in the printed specimens. Therefore, three orientations were used to study this possible property when applied to TPO, as shown in Fig. 3a. Two nozzles were used to print the specimens, namely 0.4 mm and 1 mm nozzles. The comparison of the tensile testing results will highlight any discrepancies in print strength of the specimens printed using different nozzle sizes and printing orientations. All the specimens were tested on a M350 20CT tensile tester by Testometric, United Kingdom using an LC50, 490 N load cell. The test was conducted at 500 mm/min. Each condition was tested using ten specimens.

The specimens were all printed using a printing speed of 30 mm/s for all 3D-printing features including the first layer speed. For each nozzle size used, ten specimens were printed. The layer height was set to 0.2 mm and 0.5 mm for the 0.4 mm and 1 mm nozzles, respectively. All specimens were printed without layer cooling to attain the best experiment repeatability and to ensure good layer bonding [25]. The XY specimens were printed flat on the printing bed, using 100% aligned rectilinear infill, and without perimeters. The YZ specimens for the 0.4 mm nozzle were printed directly using supports to bridge the gap. On the other hand, for the 1 mm nozzle, the printed YZ specimens were still too hot to maintain their shape adequately during printing. In light of this issue, a triangular prism blank, as shown in Fig. 3b, left was 3D printed. Similarly, both 0.4 mm and 1 mm nozzles, Z specimens were punched out of an appositely printed pentagonal prism blank, as shown Fig. 3b, right. Since TPO is an elastomer and rather soft during its solidification, it is not sufficiently stiff to provide support to directly 3D print the long and thin Z orientation specimens

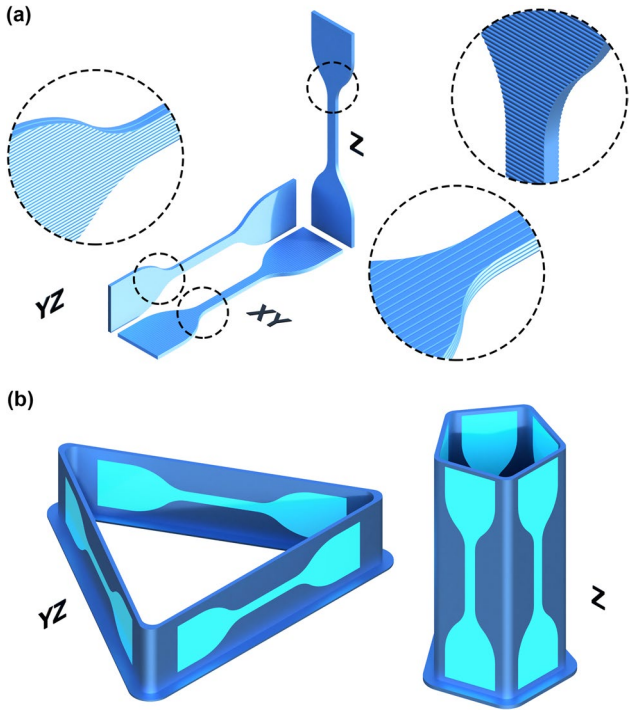

Fig. 3 **a** Tensile testing orientations for XY, YZ, and Z specimens and **b** geometry of 3D-printed blanks for YZ and Z orientations

as these would bend during 3D printing resulting in a poor-quality part. A summary of the preparation method used per case to produce the tensile specimens, is shown in Table 3

2.5.3 Dynamic mechanical analysis (DMA)

In many applications, one example being in automotive, elastomers are expected to maintain their properties in a set temperature envelope. The tensile testing experiment described above does not take this aspect into account. To remedy this deficiency, a temperature sweep, dynamic mechanical analysis (DMA) test was carried out.

The DMA test was conducted on an STAR System DMA 1 by Mettler Toledo (Ohio, USA). It was carried out in tension with the load being applied in the 3D-printing direction, i.e., perpendicular to the cross-section of the deposited strands, as shown in Fig. 4. The DMA results include the change in storage modulus (M') and Tan (δ) with temperature. The storage modulus is a measure of the energy required to distort a sample. Conversely, the loss modulus (M'') is a measure of the energy lost (dissipated) during a cycle of strain on the sample. Tan (δ) is a ratio between the loss and storage modulus, i.e., the higher the value, the more viscous the material. By assessing the change in storage modulus and Tan (δ), one can also find the T_g along with any perturbations in mechanical properties experienced and an indication of possible phase changes.

The temperature sweep DMA tests were carried out using a 10 µm amplitude, as suggested by an amplitude sweep test carried out beforehand. The temperature sweep test was set to cover a temperature range between − 100 °C and 125 °C, changing at a rate of 10 K/min and was carried out in a nitrogen atmosphere. The test was carried out twice and in each case 25 mm by 5 mm by 2 mm cuboids' specimens were used. These specimens were printed flat on the print bed at 30 mm/s, using the 1 mm nozzle with perimeters only. The test was conducted by first cooling to − 100 °C and then reheating to 125 °C.

Table 3 Preparation method for tensile testing specimens

Nozzle diameter (mm)	Orientation		
	XY	YZ	Z
0.4	As printed	As printed	Printed blanks and die cut
1.0	As printed	Printed blanks & die cut	Printed blanks and die cut

3 Results and discussion

3.1 Differential scanning calorimetry (DSC)

The DSC results presented in Fig. 5 show a typical curve of a semi-crystalline thermoplastic. The most pertinent results are summarized in Table 4. Both shoulders at − 35 °C and 79 °C refer to the secondary T_{g1} and primary T_{g2} glass transitions of TPO. The peak at 143 °C indicates the melting temperature T_m at which point the main crystal structure of the polymer is molten. The crystallization temperature T_c, when cooling at 10 K/min, occurs at about 99 °C, which marks the

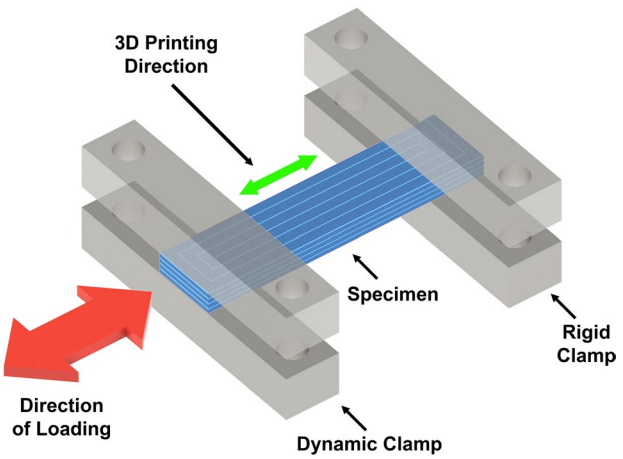

Fig. 4 Schematic diagram of DMA test with 3D-printing direction

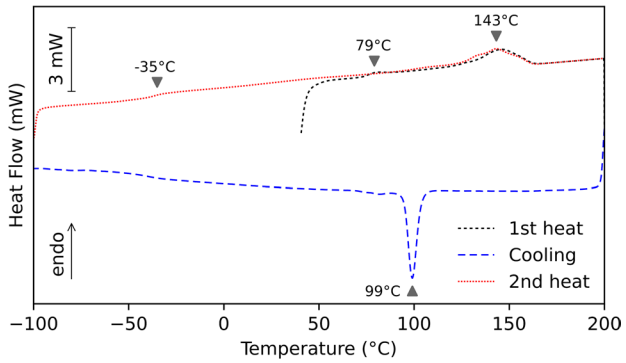

Fig. 5 DSC graph of TPO pellet samples

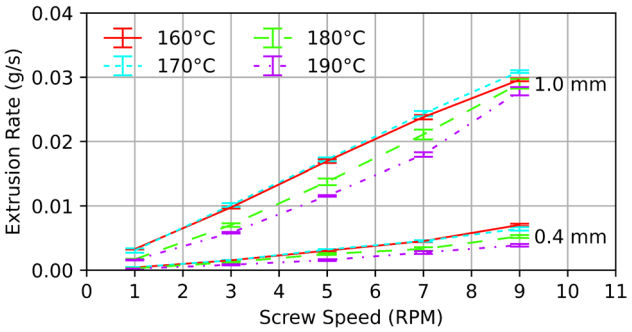

Fig. 6 Extrusion rate at varying screw speed, temperature, and nozzle size

Table 4 Summary of DSC results for Adflex X 100 G TPO

Property	Symbol	Value
Secondary glass transition temperature	T_{g1}	− 35 °C
Primary glass transition temperature	T_{g2}	79 °C
Melting temperature	T_m	143 °C
Crystallization temperature	T_c	99 °C

point at which molten material cools sufficiently to crystallize and solidify. The second heating curve presented a larger peak at the T_m region suggesting that after the first heat and cooling cycle, the crystallinity achieved was higher than in the initial pellet. This result also suggests that any melt processing using this grade of TPO should be conducted beyond 143 °C and ideally higher than about 165 °C to ensure that the crystal structure is fully molten and the viscosity gets lower, which makes it easier to process. Given that the T_{g2} was found to be 79 °C, the build plate temperature should be set at around 80 °C.

The results of the DSC indicate that TPO could be used as an elastomer even in cold, sub-zero environments. It is impractical to compare the performance of TPO to TPU in this regard as TPU is really an agglomeration of wide variety of formulations. This point is well illustrated by the work of León-Calero et al. who studied different TPU formulations and identified the relevant monomers [26]. The lower and upper glass transition temperatures vary wildly and were found to be as low as -60 °C and as high as 165 °C for different, discrete TPU formulations [26–30].

3.2 Extrusion rate analysis and calibration

The results of the extrusion rate tests are plotted in Fig. 6. As expected, the 1 mm nozzle achieved a higher extrusion rate than the 0.4 mm nozzle. There is a nearly linear relationship but not one to one between the screw speed and extrusion rate. Therefore, the FGF process requires different extrusion multipliers for different printing speeds. The extrusion rate was also significantly influenced by the barrel temperature. Increasing the barrel temperature beyond 170 °C reduced the extrusion rate. At 160 °C, the extrudate was broken and had a staggered look, since the melt temperature was too low for consistent and homogenous extrusion. Therefore, 170 °C was deemed the most suitable temperature for 3D printing with the current setup as it provided the best extrusion rate combined with a good melt flow consistency. The effects of both temperature and screw speed were the same for the 0.4 mm and 1 mm nozzles. Given that extrusion rate is influenced by screw speed, and the relationship is not one to one, any calibration done has to be carried out at constant speed. Otherwise, the extrusion rate will vary whilst printing and the calibration will be incorrect. The cube calibration was carried out at 30 mm/s using both nozzle sizes separately. For the 1 mm and 0.4 mm nozzles, the EM was found to be 0.85 and 5.5, respectively, both at 170 °C.

The extrusion rate result also allows for the determination of the maximum 3D-printing speed. Using the TPO density of 0.88 g/cm^3 as per data sheet [9] and the extrusion rate results at 9 RPM, the max-volumetric speed (MVS) was calculated for both the 1 mm and 0.4 mm nozzles. The MVS is an industrial metric which defines the max-volumetric speed of material being extruded by the extruder. The MVS was calculated to be 34.1 mm^3/s and 8.5 mm^3/s for the 1 mm and 0.4 mm nozzles, respectively. For comparison, the widely used E3D V6 filament extruder reported an MVR of about 15 mm^3/s and 2.5 mm^3/s for polylactic acid (PLA) and TPU/TPE, respectively, using the 0.4 mm nozzle [31]. Therefore, the extrusion rate of the setup provided is not only sufficient for conventional desktop 3D printing but can reach even higher speeds if provided with sufficient cooling and an adequate motion system.

3.3 Build plate adhesion

TPO did not adhere well to most common 3D-printing build surfaces. The build plate temperature was set at 80 °C for optimal adhesion, as indicated by the DSC results. The results of the build plate adhesion test are shown in Table 5, with the best performing being glass with Magigoo PP glue at 80 °C. Using this build plate setup, the 3D-printed parts adhered very well and printed without warpage. All the other build plate setups provided an inadequate bond.

The PVA glue acted as a release layer, i.e., rather than promoting a better adhesion between the part and build plate, it ensured that the extruded TPO would not adhere at all. In contrast, ABS build plate adhesion improves when using PVA glue. The Magigoo Flex surface did improve adhesion unlike with the PVA glue, but nevertheless the bond was insufficient for 3D printing. Magigoo Flex is marketed as a glue for TPUs and TPEs, which should make it adequate for TPO as it belongs to the latter polymer group. It is concluded that the most suitable glue for TPO is Magigoo PP. PP is a major component of TPO, and therefore, it makes sense that such a combination would work well and is the reason why this glue was selected for testing in the first place. The other non-adhesive methods fared rather poorly.

3.4 3D printing of complex geometries

Successful production of the curly vase model demonstrated sufficient extrusion rate consistency for AM. The 3D printed vase is shown in Fig. 7a and its flexibility is demonstrated in Fig. 7b. This result empirically proves that granulate extrusion of TPO using a screw with a low length-to-diameter (L/D) ratio as previously described is adequate for 3D printing, even when challenged with a highly flexible object such as the vase shown. The vase had no unexpected blemishes or under extrusions that would be caused by an inconsistent extrusion rate. Each curl of the vase had the same surface and pattern, which indicates that the motion system does not have any noticeable defects.

Table 5 Classification of TPO adhesion to different build surfaces

Build plate surfaces	Adhesion	
	Build plate temperature	
	RT	80 °C
Smooth Aluminum	None	Very Poor
Brushed Aluminum	Very Poor	Poor
Smooth Galvanized Steel	None	Very Poor
Brushed Galvanized Steel	Very Poor	Poor
Glass	Poor	Poor
Glass with PVA glue	None	None
Glass with PEI tape	Poor	Poor
Glass with PEI tape and PVA glue	Poor	Poor
Glass with Magigoo Flex	Poor	Good
Glass with Magigoo PP	Good	Very Good

Legend: None: No adhesion at all; Very Poor: Inconsistent bonding and poor first layer quality; Poor: Initial bonds weakly but as 3D print progresses the adhesion is insufficient; Good: Better adhesion than poor but still insufficient, long parts detach; Very Good: Part has to be pulled off the bed to be able to remove, or else the bed is left to cool

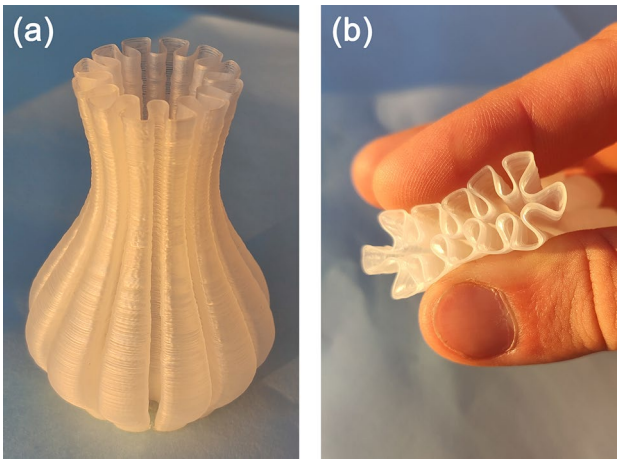

Fig. 7 Curly case, 3D printed out of TPO (**a**) and shown squashed (**b**)

The Benchy was a more challenging model to 3D print compared to the previous case study parts. This model has multiple retraction points, as shown by the red dots in Fig. 8a. Each retraction point can either be a point of stringing caused by a lower retraction value or a point of under-extrusion caused by excessive flow inhibition. Insufficient retraction leads to stringing which, in this case, would follow the green lines illustrated in Fig. 8b. Stringing which is easy to remove by hand leaves a minor blemish on the 3D-printed part and is often acceptable. Without retraction, the stringing was severe, as shown in Fig. 8c; nonetheless, the Benchy could be cleaned well and its overall quality was adequate. The best result was achieved at 3° reverse angle as the Benchy printed with good fidelity to the digital model and the amount of stringing was quite low, as shown in Fig. 8e. Increasing the reverse angle further led to under-extrusion as can be seen in Fig. 8f. Notably, the under extruded regions were mostly clustered in regions with a high density of retraction points. Therefore, a high retraction value was observed to cause under-extrusion in the subsequent lines.

The reverse angle of 3° was used when printing the gyroid egg model. The egg printed without any stringing, as shown in Fig. 9b, c. The retraction point diagram of the gyroid egg, shown in Fig. 9a, indicated that the model is widely populated with retraction points, but that these are

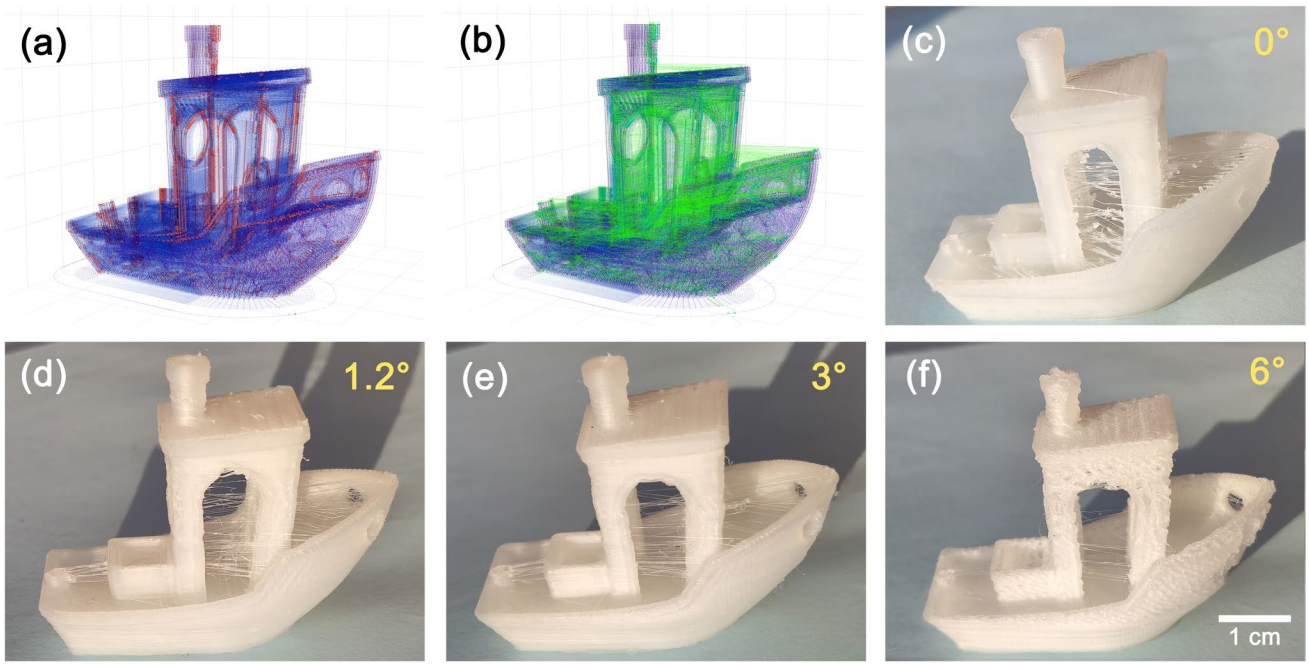

Fig. 8 Retraction diagram of Benchy where in (**a**), the red dots represent the retraction points, and in (**b**), the green lines are the travel movements after retraction. The 3D-printed Benchys using 0° (**c**), 1.2° (**d**), 3° (**e**), and 6° (**f**) reverse screw rotation on retraction

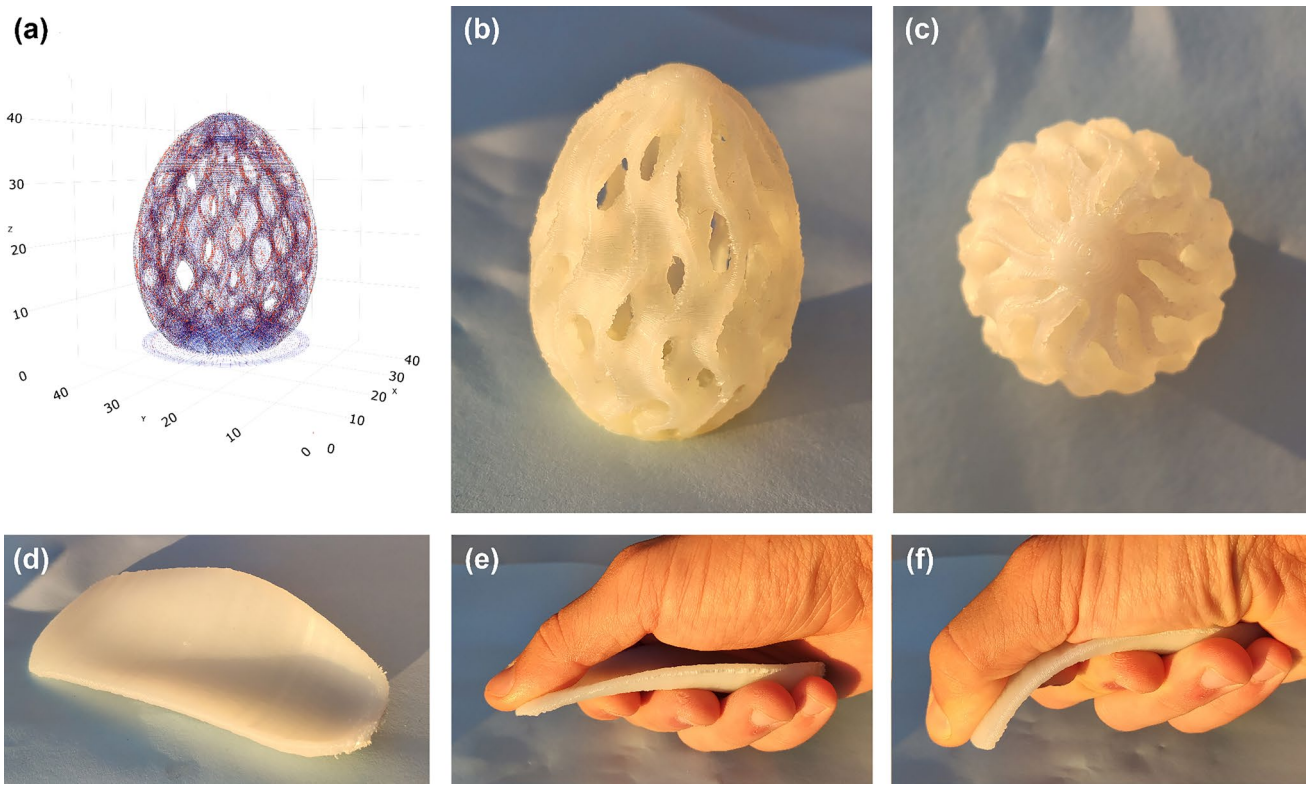

Fig. 9 Retraction diagram of gyroid egg where in (**a**), the red dots represent the retraction points and blue lines are the 3D-printing path. The 3D-printed gyroid egg from side (**b**) and top (**c**). Orthotic insole 3D printed out of TPO (**d**) shown straight (**e**) and bent (**f**)

well distributed throughout the model. In fact, the edges of the gyroid egg were found to be rather rough as they were dotted with seemingly random, tiny blobs of over extruded TPO. When select zones were compared with the retraction point diagram, it was confirmed that these blobs were located at the ends of discrete perimeters. To remedy this issue, the extruder should have been set with a marginally higher reverse angle to account for this blobbing.

The last 3D-printed model was the orthotic insole shown in Fig. 9d. The insole was printed rather small, more adequate for a child's size. The surface was printed smooth and without blemishes. The insole was pliable but required some effort to bend in the fashion shown in Fig. 9e, f. Upon bending, the insole did not crack or tear; nonetheless, further studies would be required for a practical application to determine the longevity of the layer bond when bent repeatedly.

3.5 Water uptake

The results of the water absorption test are shown in Fig. 10 along with the Fick's Law fitted curve. The water content at saturation, c_s, was found to be 0.25% mass gain. The diffusion coefficient, D, was calculated to be 1.79×10^{-6} cm^2/s. The results fitted well with Fick's law, indicating that Fickian diffusion applies. The overall level of water uptake was lower than that gained by most TPU filaments used in 3D printing. Bruère et al. reported a water uptake of almost 2% which is about eight times that reached by TPO. Some TPO manufacturers, such as The Plastic Group of America, recommend that pre-drying is not required for TPO [32]. During the use of the 3D-printing system, the extruder did not have any perceivable difference in extrusion rate, aesthetic and dimensional accuracy when using undried TPO granules.

3.6 Tensile testing

The tensile testing results are listed summarily in Fig. 11, with representative curves of each specimen type in Fig. 11a.

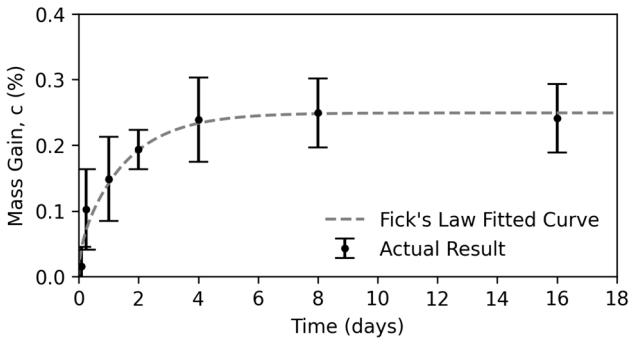

Fig. 10 Measured water absorption and Fick's law fitted result

The results were represented as box plots with average lines in Fig. 11b–d with dots representing statistical outliers. An independent sample t test was also conducted to determine whether the average result of the same orientation but with different nozzle sizes, are equivalent. The p value of each result is shown in Fig. 11b–d, where a value under 0.05 means that with a 95% confidence, the averages are not equivalent. The properties of the same material, taken from its material data sheet [9], are represented as a dashed line in Fig. 11b–d. In the case of the strain at break value, the data sheet provides only a lower limit instead of a definite value. The following comparisons are made with the values from the material datasheet as it is the only source available for the exact same grade used in this study. Since the values in the material datasheet are obtained from injection molded parts, such comparisons highlight the strengths and weakness of this relatively new FGF process as opposed to the well-established injection molding process. The only other similar source available is the research work published by Adrover-Monserrat et al. [5], but the material grade used was not the same; therefore, a comparison is not warranted.

Across both 1 mm and 0.4 mm nozzle specimen types, the Z orientation specimens were the weakest in all metrics studied. The XY orientation test results for both 1 mm and 0.4 mm nozzles achieved the highest average stress at yield. The best average result was achieved by 0.4 mm nozzle, XY orientation, coming at 6.36 MPa. When it comes to stress and strain at break, the results of the XY and YZ orientations are rather similar except for the YZ orientation, 1 mm results. This orientation and nozzle size topped the chart, with an average stress at break of 13.8 MPa and strain at break of 1300%.

The YZ specimens, 3D printed using the 1 mm nozzle were a clear outlier when considering stress and strain at break. This was most probably caused by the die cutter used to cut the shape of the tensile specimens rather than printing them directly. In contrast to directly printed specimens, the edges and shape of the die cut specimens did not have any discontinuities or blemishes. The directly 3D-printed specimens, i.e., those using the 0.4 mm nozzle, YZ orientation, inherently have edge discontinuities. These discontinues are caused by the bridging and support structure required to 3D print such specimens. Any imperfection in the specimen then acts as tear initiator during the tensile testing process, leading to a lower attainable stress and strain at break. Going back to the die cut, 1 mm nozzle specimens, the high stress and strain at break achieved was caused by strain hardening.

Both the stress at break and strain at break results of the 1 mm nozzles were always higher than their 0.4 mm counterpart. All specimens were printed with a half nozzle diameter layer height, i.e., 0.2 mm and 0.5 mm for the 0.4 mm and 1 mm nozzles, respectively, and therefore, the discrepancy should not be accounted towards that. The

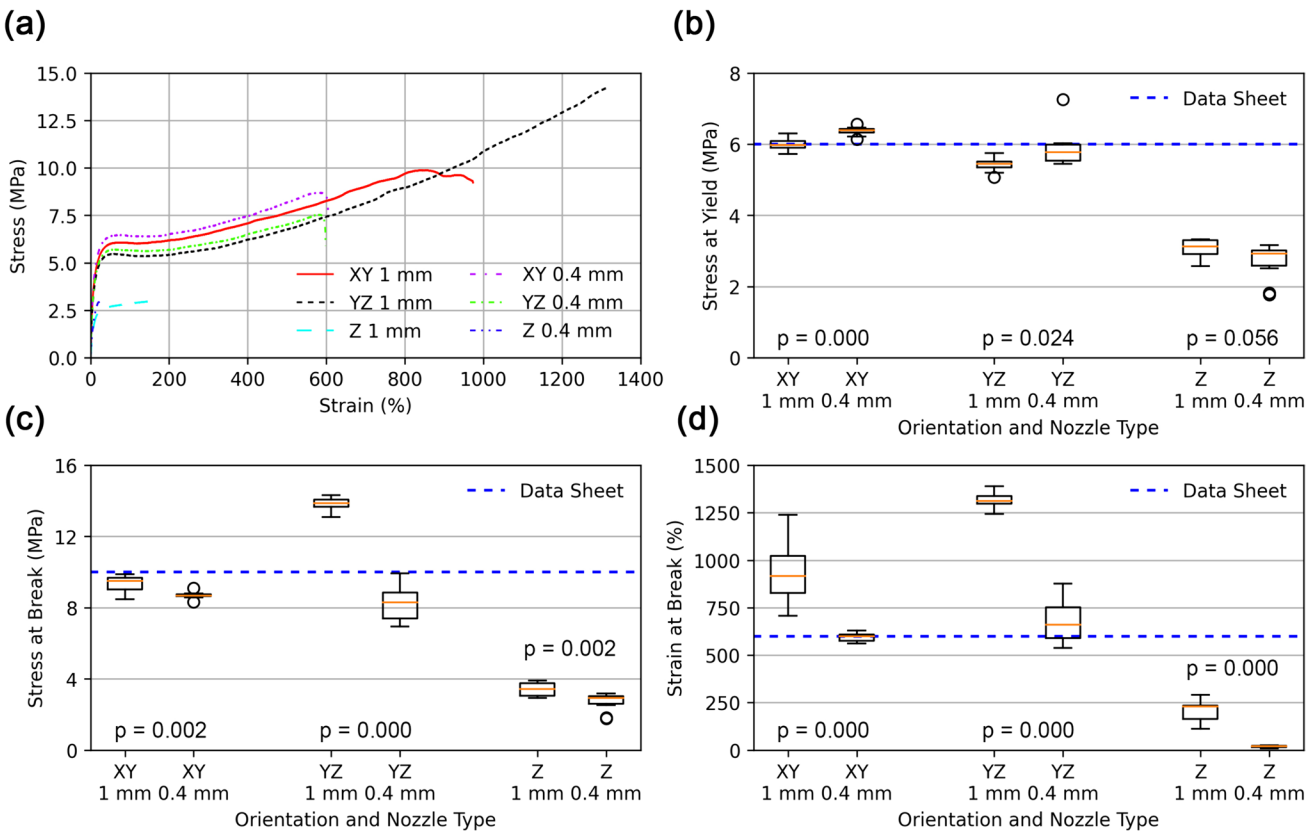

Fig. 11 Representative results of tensile test (**a**), stress at yield (**b**), stress at break (**c**), and strain at break (**d**) with average result line and data sheet value line for comparison ($n = 10$). The circles represent statistical outliers in the results. The p value is the result of an independent sample t test, $p < 0.05$ confirms the hypothesis that the averages are not the same with a 95% confidence

discrepancy is also non-trivial, as attested by the low p value of the sample t test carried out between the 1 mm and 0.4 mm nozzle results. The difference is often stark, especially when considering strain at break, where specimens printed using the 1 mm nozzle reached significantly higher values, often around double their 0.4 mm nozzle counterparts.

It was postulated that the changes in mechanical properties observed were caused by the differences in bond strength. This could be attributed to the higher energy content in 1 mm strands as opposed to 0.4 mm strands. All specimens were 3D printed without cooling to ensure that the experiment is easily reproducible given that there is no standard airflow rating. This decision may have exacerbated the energy level difference between the two nozzle sizes. If the cross-sectional area of the two is considered, the area of the 1 mm extruded strand is more than six times higher than that of the 0.4 mm strand. Therefore, the 1 mm strand has a greater amount of energy available for material diffusion with the underlying layer, thus leading to a stronger bond. This effect might explain the improved stress at break and elongation of the 1 mm nozzle, specimens. This improvement was not reported when it comes to yield strength results; rather, the 0.4 mm nozzle specimens had a slightly higher yield strength for XY and YZ specimens.

Unlike the stress and strain at break, the stress at yield is rather similar for all orientations and is not affected as much by any defects in the specimens. Nonetheless, the Z orientation specimens fared poorly in all three properties, as is generally the case with MEX AM [33]. The nozzle diameters did not affect the stress at yield as the p value indicates that the average result of the two nozzle sizes is equivalent. The Z orientation strength is lower than that of the other orientations, since these have a higher void volume resulting in a lower contact area. The 3D-printed strand orientation also contributes to the Z specimen strength. For both XY and YZ orientations, the load is parallel with the 3D-printing direction, thus ensuring maximal strength. Finally, Z orientation specimens, by design, are susceptible to under-extrusion event. An under-extrusion event can be either a slight dip in extrusion rate over a period of time or a sudden, significant decrease in extrusion rate for a short period of time. In either case, for XY and YZ orientation specimens, the weakened zone would always be parallel with the load, whereas for Z orientation specimens, it would be perpendicular, as shown in Fig. 12, and it could affect all the cross-sectional area

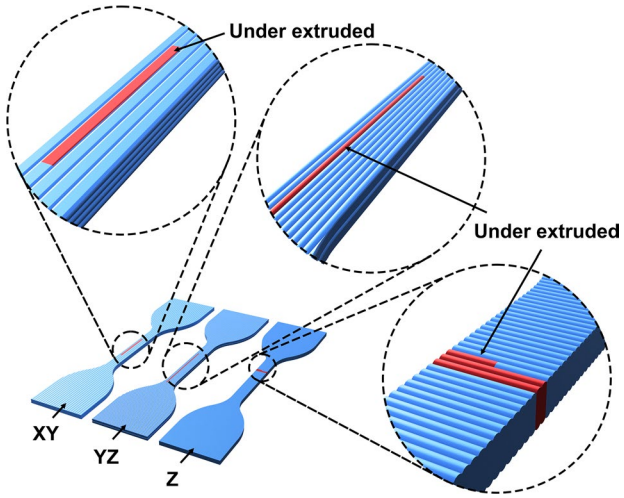

Fig. 12 Schematic diagram of possible location of under extruded strand/zone

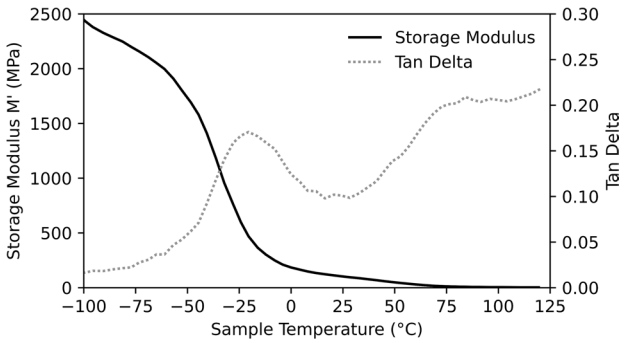

Fig. 13 DMA results of TPO showing storage modulus M' and Tan(δ) against temperature

under load or a significant amount of it. This indicates that not only is the Z orientation weaker it may also be more prone to defects caused by under-extrusion or any similar extrusion deficiencies.

3.7 Dynamic mechanical analysis (DMA)

The DMA conducted on the TPO specimens, shown in Fig. 13, demonstrated how glassy the material becomes at sub-zero temperatures. At − 100 °C, TPO becomes somewhat stiffer than ABS at room temperature [34, 35], reaching an M' of nearly 2500 MPa. At temperatures higher than about − 23 °C, most of the stiffness is lost and the material becomes elastomeric. This observation is supported by the low storage modulus and the peaking Tan (δ). Heating beyond 70 °C softens the material further and makes it act more viscous rather than elastic. At this point, the TPO was found to have a very low stiffness. Therefore, TPO may be used as an elastomer with a temperature range between − 23 °C and 70 °C.

The DMA results of TPO are difficult to compare with those of TPU for the same reason as when trying to compare DSC results. TPU is a varied material with tunable properties depending on the composition used. Even when it comes to how stable the storage modulus is within a set temperature range, some TPU formulations such as that studied by Beloshenko et al. and Harynska et al. are rather stable, seemingly more so that the TPO results presented here [29, 36]. Others, such as the formulations studied by Shin et al. and Maldonado et al. were rather unstable, with a decreasing storage modulus with temperature [37, 38].

4 Conclusion

TPO was proven to be suitable as a thermoplastic elastomer (TPE) for screw-based material extrusion (MEX) additive manufacturing (AM). Fused granulate fabrication (FGF) using TPO achieved satisfactory results to generate complex parts of high quality such as the Benchy and child orthotic insole. The measured water content saturation (c_s) of around 0.25% is considered as low and is eight times lower than the one of TPU. This suggests that TPO most likely does not require drying before use. This is a crucial advantage over the dominant MEX elastomer TPU.

The DSC and extrusion rate results revealed that TPO extrudes best at 170 °C barrel temperature. The extrusion rate and screw speed did not have a one-to-one relationship; therefore, the speed must be kept constant throughout. For the 1 mm and 0.4 mm nozzles, both at printing speed and temperature of 30 mm/s and 170 °C, the optimal extrusion multiplier was found to be 0.85 and 5.5, respectively. TPO was found to adhere best to glass at 80 °C when using Magigoo PP glue.

Additively manufactured TPO was found to be anisotropic, with the XY and YZ orientations achieving superior stress at yield as well as stress and strain at break than the Z orientation. The best average stress at yield of 6.36 MPa was achieved when using the 0.4 mm nozzle and XY orientation, whereas the best average stress and strain at break of 13.8 MPa and 1300%, respectively, were reached by the specimens printed in the YZ orientation using the 1 mm nozzle. The DSC results of TPO indicated that a glass transition temperatures (T_{g1}) occurs at − 35 °C and the (T_{g2}) at 79 °C, with melting (T_m) at 143 °C and crystallization (T_c) at 99 °C. The DMA experiments confirmed these results and reported that the working elastomeric temperature range of FGF TPO is − 23 °C and 70 °C.

The results of this study attest to the applicability of TPO as a thermoplastic elastomer for material extrusion 3D printing.

Acknowledgements The authors would like to thank all partners involved in the MALTI3D project for their continuous support.

Author contributions AC: conceptualization, methodology, software, formal analysis, investigation, data curation, writing—original draft preparation, writing—reviewing and editing, and visualization. AR: conceptualization, methodology, formal analysis, investigation, resources, writing—reviewing and editing, supervision, project administration, and funding acquisition. AG: methodology, resources, writing—reviewing and editing, supervision, and project administration.

Funding Open Access funding provided by the University of Malta. The research leading to these was part of the MALTI3D research project, which was funded by the Malta Council for Science and Technology through the FUSION: R&I Technology Development Programme (R&I-2018-009T).

Data availability Data will be made available on request.

Declarations

Conflict of interest On behalf of all authors, the corresponding author states that there is no conflict of interest.

References

1. Zanchin G, Leone G (2021) Polyolefin thermoplastic elastomers from polymerization catalysis: advantages, pitfalls and future challenges. Prog Polym Sci 113:101342. https://doi.org/10.1016/j.progpolymsci.2020.101342
2. Akkapeddi MK (2003) Commercial Polymer Blends. In: Utracki LA (ed) Polymer Blends Handbook. Springer, Netherlands, Dordrecht, pp 1023–1115
3. Laoutid F, Lafqir S, Toncheva A, Dubois P (2021) Valorization of Recycled Tire Rubber for 3D Printing of ABS- and TPO-Based Composites. Materials 14:. https://doi.org/10.3390/ma14195889
4. Lv Q, Peng Z, Meng Y et al (2022) Three-dimensional printing to fabricate graphene-modified polyolefin elastomer flexible composites with tailorable porous structures for electromagnetic interference shielding and thermal management application. Ind Eng Chem Res 61:16733–16746. https://doi.org/10.1021/acs.iecr.2c03086
5. Adrover-Monserrat B, Llumà J, Jerez-Mesa R, Travieso-Rodriguez JA (2023) Mechanical characterization of thermoplastic elastomers based on olefin processed through material extrusion. Int J Adv Manuf Technol 127:323–333. https://doi.org/10.1007/s00170-023-11523-w
6. Drobny JG (2014) Handbook of Thermoplastic Elastomers, 2nd ed. Elsevier B.V.
7. Bruère VM, Lion A, Holtmannspötter J, Johlitz M (2022) Under-extrusion challenges for elastic filaments: the influence of moisture on additive manufacturing. Prog Addit Manuf 7:445–452. https://doi.org/10.1007/s40964-022-00300-y
8. Hailat M, Xiao HX, Frisch KC (2000) Studies on the modification of thermoplastic polyolefins (TPOs)—Part I. effect of various modifiers on the adhesion of a two-component (2K) polyurethane coating to the modified TPOs. J Elastomers Plast 32:194–210. https://doi.org/10.1177/009524430003200302
9. Adflex X100G—Technical Datasheet. In: LyondellBasell. https://www.lyondellbasell.com/en/polymers/p/Adflex-X-100-G/cec1080a-3998-4cb1-85bd-616155008e33. Accessed 15 Dec 2023
10. Elastollan® (TPU)—the thermoplastic polyurethane of BASF. https://plastics-rubber.basf.com/emea/en/performance_polymers/products/elastollan.html. Accessed 15 Dec 2023
11. Massey LK (2002) Permeability Properties of plastics and elastomers a guide to packaging and barrier materials, 2nd ed. Elsevier B.V.
12. Pracella M (2017) 7—Blends and Alloys. In: Jasso-Gastinel CF, Kenny JM (eds) Modification of polymer properties. William Andrew Publishing, pp 155–184
13. Ryntz RA (2000) Paintable, surface-damage resistant reactor grade thermoplastic olefin (TPO)
14. Kumar N, Kumar Jain P (2021) Analysing the influence of raster angle, layer thickness and infill rate on the compressive behaviour of EVA through CNC-assisted fused layer modelling process. Proc Inst Mech Eng C J Mech Eng Sci 235:1731–1740. https://doi.org/10.1177/0954406219889076
15. Kumar N, Jain PK, Tandon P, Mohan Pandey P (2018) Experimental investigations on suitability of polypropylene (PP) and ethylene vinyl acetate (EVA) in additive manufacturing. Mater Today 5:4118–4127. https://doi.org/10.1016/j.matpr.2017.11.672
16. Kumar N, Jain PK, Tandon P, Pandey PM (2018) Extrusion-based additive manufacturing process for producing flexible parts. J Braz Soc Mech Sci Eng 40:143. https://doi.org/10.1007/s40430-018-1068-x
17. Leng J, Wu J, Chen N et al (2019) The development of a conical screw-based extrusion deposition system and its application in fused deposition modeling with thermoplastic polyurethane. Rapid Prototyping J 26:409–417. https://doi.org/10.1108/RPJ-05-2019-0139
18. Khondoker MAH, Sameoto D (2019) Direct coupling of fixed screw extruders using flexible heated hoses for FDM printing of extremely soft thermoplastic elastomers. Prog Addit Manuf 4:197–209. https://doi.org/10.1007/s40964-019-00088-4
19. Curmi A, Rochman A (2023) Miniaturized fused granulate fabrication of polyether ether ketone (PEEK). Prog Addit Manuf. https://doi.org/10.1007/s40964-023-00518-4
20. Rauwendaal C (2014) Polymer extrusion, 5th ed. Hanser Publications
21. Tadmor Z, Gogos CG (2006) Principles of Polymer Processing, 2nd Edition | Wiley, 2nd edn. Wiley-Interscience
22. Spoerk M, Gonzalez-Gutierrez J, Sapkota J et al (2018) Effect of the printing bed temperature on the adhesion of parts produced by fused filament fabrication. Plast, Rubber Compos 47:17–24. https://doi.org/10.1080/14658011.2017.1399531
23. #3DBenchy. In: #3DBenchy. https://www.3dbenchy.com/. Accessed 15 Dec 2023
24. Thingiverse.com Ten Easter Eggshells by DaveMakesStuff. https://www.thingiverse.com/thing:5316996. Accessed 15 Dec 2023
25. Lee C-Y, Liu C-Y (2019) The influence of forced-air cooling on a 3D printed PLA part manufactured by fused filament fabrication. Addit Manuf 25:196–203. https://doi.org/10.1016/j.addma.2018.11.012

26. León-Calero M, Reyburn Valés SC, Marcos-Fernández Á, Rodríguez-Hernandez J (2021) 3D Printing of thermoplastic elastomers: role of the chemical composition and printing parameters in the production of parts with controlled energy absorption and damping capacity. Polymers 13:. https://doi.org/10.3390/polym13203551
27. Rigotti D, Dorigato A, Pegoretti A (2018) 3D printable thermoplastic polyurethane blends with thermal energy storage/release capabilities. Mater Today Commun 15:228–235. https://doi.org/10.1016/j.mtcomm.2018.03.009
28. Arifvianto B, Iman TN, Prayoga BT et al (2021) Tensile properties of the FFF-processed thermoplastic polyurethane (TPU) elastomer. Int J Adv Manuf Technol 117:1709–1719. https://doi.org/10.1007/s00170-021-07712-0
29. Beloshenko V, Beygelzimer Y, Chishko V et al (2021) Mechanical properties of flexible TPU-based 3D printed lattice structures: role of lattice cut direction and architecture. Polymers 13:2986. https://doi.org/10.3390/polym13172986
30. Kabir S, Kim H, Lee S (2020) Physical property of 3D-printed sinusoidal pattern using shape memory TPU filament. Text Res J 90:2399–2410. https://doi.org/10.1177/0040517520919750
31. Max volumetric speed | Prusa Knowledge Base. https://help.prusa3d.com/article/max-volumetric-speed_127176. Accessed 15 Dec 2023
32. (2020) The Plastics Group of America. Polifil® TPO—Thermoplastic Polyolefin (Filled and Unfilled)—Processing Guide
33. Gordelier TJ, Thies PR, Turner L, Johanning L (2019) Optimising the FDM additive manufacturing process to achieve maximum tensile strength: a state-of-the-art review. Rapid Prototyping J 25:953–971. https://doi.org/10.1108/RPJ-07-2018-0183
34. Zhang S-U, Han J, Kang H-W (2017) Temperature-dependent mechanical properties of ABS parts fabricated by fused deposition modeling and vapor smoothing. Int J Precis Eng Manuf 18:763–769. https://doi.org/10.1007/s12541-017-0091-7
35. Torrado AR, Shemelya CM, English JD et al (2015) Characterizing the effect of additives to ABS on the mechanical property anisotropy of specimens fabricated by material extrusion 3D printing. Addit Manuf 6:16–29. https://doi.org/10.1016/j.addma.2015.02.001
36. Haryńska A, Carayon I, Kosmela P, et al (2020) Processing of Polyester-Urethane Filament and Characterization of FFF 3D Printed Elastic Porous Structures with Potential in Cancellous Bone Tissue Engineering. Materials 13:. https://doi.org/10.3390/ma13194457
37. Jung YS, Woo J, Lee E et al (2022) Synthesis and properties of bio-based thermoplastic poly(ether urethane) for soft actuators. J Polym Res 29:521. https://doi.org/10.1007/s10965-022-03375-x
38. Maldonado MP, Pinto GM, Costa LC, Fechine GJM (2022) Enhanced thermally conductive TPU/graphene filaments for 3D printing produced by melt compounding. J Appl Polym Sci 139:e52405. https://doi.org/10.1002/app.52405